NONDESTRUCTIVE EVALUATION

1. Introduction

The technology of nondestructive evaluation (NDE) includes all nondamaging or nonintrusive methods for determining material identity; for evaluating material properties, composition, structure, or serviceability; and for detecting discontinuities and defects in materials. Nondestructive tests commonly are used for quality control, process control, and for reliability assurance of materials, protective coatings, components, welds, assemblies, structures, and operating systems. The use of these tests helps prevent premature failure of materials during processing, manufacturing, or assembly, and during service under anticipated operating stresses and environments. Proper testing can lower manufacturing and operating costs, minimize insurance risks, and help prevent interruptions of service and potential disasters that might cause loss of life or usefulness of expensive facilities.

Nondestructive tests differ from methods of laboratory analysis and testing where specimens are generally sectioned, broken, damaged, or destroyed. Nondestructive tests can be performed on materials, components, and structures or systems that actually are to be used. Thus, effective use of NDE requires engineering knowledge of the structure, the performance characteristics, and service environment, as well as the test method. More complete information on all of the topics discussed herein are available elsewhere (1–8).

Operating companies and regulatory agencies have a vital responsibility for specifying and managing the use of nondestructive testing during erection and service of costly facilities and systems such as chemical plants, petroleum refineries, off-shore drilling platforms, nuclear power plants, and transport systems where failures during services are potentially disastrous. Effective in-service nondestructive tests of materials and additional nondestructive tests made during maintenance shutdown periods can permit early detection and subsequent correction of hidden damage or deterioration. Such test programs provide protection for the public, as well as for corporations and management from failure costs and penalties, which can include high litigation and insurance costs (9–12).

Nondestructive tests applied to consumer products ensure safety and proper operation for the purchaser. Tests might also be used periodically by the consumer during service to determine whether deterioration or conditions that might lead to premature failure have developed as a result of improper handling or storage, or misuse or abuse by operators. Inspection is especially important in cases where cracking or failure has already begun but has not progressed to the point of propagating toward a disastrous sudden failure. Use of NDE can add to customer satisfaction, eliminate the need for recalls and repairs, and help to protect both manufacturers and service industries from damage suits and litigation. The proper use of nondestructive tests can be a factor of economic survival for organizations manufacturing and servicing consumer products (9–12).

In this article a number of NDE techniques, such as liquid penetration, radiography, ultrasonics, holography, moire interferometry, eddy current, magnetic flux leakage, and thermal techniques are briefly reviewed. Advantages and

disadvantages of these techniques are discussed. A recently developed new NDE technique using guided waves is discussed in more detail. Some basic equations are presented so that the readers can understand and appreciate the experimental and theoretical results that are presented here. A comprehensive list of references is provided to help those readers who want to study more on the topics of their interest.

2. History

Nondestructive testing of materials has been practiced for many years. When someone visually inspects an object for irregularities then he/she carries out a nondestructive testing of the object. Since the visual inspection technique is many centuries old we can say that the NDE technique is also many centuries old and it is older than the destructive testing techniques. However, one should keep in mind that although the visual inspection technique is an old method most of the sophisticated NDE techniques that are practiced today are relatively new and many of these techniques have been developed in the later part of the twentieth century.

There are many NDE techniques available today for characterizing different types of materials used in engineering, medical, and bioscience applications. A partial list of these techniques include visual inspection, liquid penetration, acoustic emission, conventional ultrasonics, acoustic microscopy, atomic force microscopy, optical/electronic/tunnel microscopy, photoelasticity, optical holography, acoustical holography, moire interferometry, laser speckle interferometry, thermal shearography, X-radiography, gamma radiography, neutron radiography, tomography, nuclear magnetic resonance (nmr), magnetic field perturbation or magnetic flux leakage, eddy current method, chemical methods, microwave technique, and guided wave technique. However, even this big list does not cover all NDE techniques. Naturally, no one can be an expert of all these NDE techniques and it is impossible to describe all these methods in one chapter. Here some of the traditional NDE methods are briefly described and a relatively new ultrasonic technique based on guided waves that has good potential for pipe and chemical plant inspection are described in more detail.

3. Principles

Most nondestructive tests require external energy source and are known as active nondestructive tests. These tests also need suitable probing media to cause the test objects to emit signals that can be detected and interpreted in terms of material properties or defects. These resultant test signals may be converted to visible or audible indications, analogue electrical signals, meter or digital display readings, computer data, or images of many different types. Output signals, images, or data must then be evaluated by the human test operator or by automated test systems. Each type of probe used in active nondestructive test systems has specific capabilities and limitations. The probe type, ie, a coil, slender probe, or flat transducer, affects the response from the discontinuity or

feature to be evaluated. For example, surface, near-surface, surface-connected, interior, back-surface, flat surface, curved surface, rough or smooth surface anomalies and discontinuities such as cracks, porosity, inclusions, lamination, segregation, leaks, bonding, corrosion pinholes or attack, erosion, wall thinning, missing components, etc, all can be detected using NDE. No single type of inspection method, however, is adequate to detect all of the material conditions and discontinuities that can influence the serviceability of materials or systems. Thus, for reliable testing, two or more basically different types of test methods are usually necessary to detect and confirm conditions that may affect performance. Different materials or test-object geometries may require totally different tests or combinations of tests to ensure reliability. In many cases, the test methods appropriate for materials identification and selection prior to processing or welding are quite different from those that should be used after manufacture, erection, or during maintenance shutdown periods of facilities. In particular, the test method should be selected with consideration of materials, shapes, accessibility, and conditions or defects that affect the integrity and serviceability of the material, component, structure, or system to be tested.

Passive nondestructive tests are those for which no specific probing medium, other than environmental or service loading conditions, need be applied to test objects to obtain test signals. Signals are emitted when changes in internal stress distributions, phase or structure, temperature, corrosion attack, external loading, or other operating conditions produce them. One dramatic example of a passive signal is the loud bang that accompanies the failure of a weld or beam when it is overloaded or fails by virtue of defects. Smart materials containing embedded sensors, may be effective for passive tests.

4. Commonly Used Techniques

A brief review of commonly used NDE techniques is given in this section. Interested readers can read more about these techniques from the references provided.

4.1. Visual Inspection Method. Visual inspection is the oldest nondestructive testing method and in the opinion of many industries 80% of the defects found are located by visual inspection (1). Visual inspections are often used to detect potential abnormalities in an object. Then more sophisticated techniques are used to obtain the size and exact location of the defect. However, there is always a large degree of uncertainty associated with the visual inspection technique. Reliability of this technique depends on the minimum allowable defect size among other factors. Yonemura (13) measured the uncertainty for a single observer, between observers, and between groups of observers and concluded “No matter how consistent an inspector may be repeating his performance day after day, unless his performance meets some minimum specified performance level, the performance is unacceptable”.

Visual inspection is simple, fast, and economic. That is why an object is generally visually inspected before other more sophisticated NDE methods are used. The primary disadvantage of visual inspection is that the small defects and internal defects in an opaque object cannot be detected by this technique.

4.2. Liquid Penetrant Testing. Liquid penetrant testing is a nondestructive testing technique for detecting surface discontinuities in solid materials. Cracks and porosity open to the surface can be found by this technique. The penetrant is drawn into very small openings of cracks and pores by capillary action when it is applied to the surface of the object. After adequate dwell time, all of the excess liquid is removed from the surface. Then a powder is applied on the surface. The powder absorbs the residual penetrant from the surface cracks. Thus it gives a clear visual indications of surface discontinuities. A major advantage of this technique is that shape, size, or other geometric factors of test objects are not too important. However, it is only a surface inspection method and integrity inside the material cannot be assessed by this technique. Detail descriptions on this technique can be found in Refs. (2,14,15).

4.3. Radiography. Radiography is an effective nondestructive testing method for detecting internal flaws of a material. A radiographic image is a two-dimensional (2D) distribution of the intensity of γ-rays, X-rays, or neutrons that have passed through the material. The object attenuates the radiation according to the mass, type, and size of internal defects. Thus a radiographic image shows the distribution of internal flaws of a material. One advantage of radiography over other NDE techniques is that a wide range of material thickness levels can be assessed, extending from thin metal foils and slices of bonding materials to perhaps a foot of steel and several feet of solid rocket propellant material (1). Complex shapes can be radiographed if both sides of the material are accessible, on one side the source and on the other side the recording plate are placed. Different kinds of metallic and nonmetallic materials can be radiographed. However, the disadvantages of this technique are that radiation is a health hazard, it is expensive, mainly due to the use of a silver halide film for recording the image, some processing time is needed before the image can be seen and analyzed, delaminations and cracks perpendicular to the propagating beam are almost always undetectable. Based on what kind of beam is passed through the material, the radiography techniques can be classified into three groups, X-radiography, γ-radiography, and neutron-radiography.

X-rays are a form of electromagnetic radiations that, due to their very short wavelengths, can penetrate materials that are opaque to light. X-rays are capable of ionizing photographic films and forming latent image, which are later developed. However, X- and γ-rays are also capable of ionizing human tissues also and thus are considered health hazards. X-rays are generated by highvelocity electrons striking a metallic target, which, in the flaw detection X-ray system, is usually tungsten embedded in copper. γ-Rays differ from X-rays in their source. While X-rays are electromagnetic waves generated electrically, γ-rays are emitted while artificial and naturally occurring isotopes decay. Isotopes that are capable of generating γ-rays are Co 60, Ce 137, Ir 192, and Th 170. For half-life and penetration capabilities of these isotopes, and a more elaborate description of the X-radiography and γ-radiography the readers are referred to Refs. (1,8,16).

In neutron-radiography or N-radiography neutrons are used instead of X- or γ-rays for penetrating the materials. Neutrons can be obtained from nuclear reactors, from particle accelerators, from artificially produced radioactive sources, from spontaneous fission of isotopes, and by subcritical neutron multiplications. Neutrons interact with the atomic nucleus, and their attenuation

is proportional to material density and neutron absorption of the cross-section while X-rays interact with atomic orbiting electrons, and X-ray attenuation is proportional to material density and atomic number. Consequently, one method cannot replace the other, they complement each other. A detailed description of neutron or N-ray detection techniques can be found in Ref. (17).

4.4. Magnetic Resonance Testing. Magnetic resonance is found in systems that possess magnetic moments and angular momenta (18). Nuclear magnetic resonance and electron paramagnetic resonance (epr) spectroscopies are the two main types of magnetic resonance testing techniques that have been used in the past by chemists and molecular physicists to study intra- and intermolecular structures and reaction mechanisms. Nuclear magnetic resonance was discovered in 1945. Since then it has become a major tool for the investigation of the microscopic structure and properties of matter. This techniqes is useful for determining molecular structure and for monitoring chemical reaction mechanisms and rates without affecting the structure, mechanism, or rates of the material or reaction being investigated. Nuclear magnetic resonance has been used in medical imaging in a manner similar to X-ray computed axial tomography (19). However, nmr imaging uses no ionizing radiation and thus it is nonhazardous. Outside the medical field nmr has been used for detecting explosives in packages and for determining moisture content of the composite materials (20). Both epr and nmr techniques are very similar, the main difference is that epr is microwave induced and nmr is radio-frequency (r-f) induced transitions of magnetic energy levels of atomic nuclei. Electron paramagnetic resonance is particularly useful for determining molecular structures and monitoring chemical reactions without affecting the samples being examined. Out of these two techniques so far only nmr has been used as an imaging tool. For a more detailed description of nmr principles and applications readers are referred to Ref. (21).

4.5. Magnetic Flux Leakage Technique. Static magnetic fields are used widely to test ferromagnetic materials for surface and near-surface defects (1,2,5-8). Steels and other ferromagnetic materials are strongly magnetized using external coils, yokes, or magnets. The relationship between elctric current and magnetic field directions is described by the right-hand rule, with the thumb of the right hand in the current direction and the fingers in the direction of the field lines. Circular magnetization of tubes or round bars is done by passing a high direct current (dc) or alternating current (ac) magnetizing current through a central conductor or through the test object itself. Longitudinal fields are generated in round parts such as bars and tubes by inserting them in an energized circular coil. Additionally, magnetic yokes having movable legs are used to excite longitudinal fields in both flat and irregularly shaped parts. Flux lines in a saturated ferromagnetic material are diverted by cracks, loss of wall thickness, or other anomalies, so that these flux lines leak into the surrounding medium, as shown in Figure 1.

Two quantities H and B are necessary to describe a magnetic field. They are related in the following manner:

$$B = \mu_0(H + M) = \mu_r \mu_0 H \tag{1}$$

where μ_0, the permeability in a vacuum, $= 4\pi(10^{-7})$ henries H/m, $\mu_r =$ relative permeability, $H =$ field strength or field intensity (in amp/m), M is the intensity of magnetisation in the material, $B =$ magentic flux density $= \Phi/A$ (in teslas T), $\Phi =$ total flux (in Wb), and $A =$ area (in m^2). Other parameters useful in defining the magnetic response of a material are the saturation flux density, B_s; remanence or retentivity, B_r; and the coercive force, H_c.

The magnetic leakage field may be detected in several ways, most frequently by a moving conducting coil or sensor, very fine ferromagnetic particles, or recording tape. A moving probe coil or a semiconductor magnetic field detector passing through a leakage field causes a voltage to be generated. The voltage may be analyzed to determine the presence and characteristics of typical defects. Finely divided, low remanence magnetic particles are another common technique for indicating flaws. When these particles are applied to the surfaces of the suitably magnetized test object, they collect where magnetic flux leakage exists at the material surface. These accumulations usually define cracks, porosity, or near-surface submerged cavities. The particles may be coated with lubricants and color dyes or fluorescent materials to aid visibility. Parts tested using visible dye coatings are inspected under white light; those tested using fluorescent magnetic particles are inspected under near-ultraviolet (uv) radiation (365 nm) from a filtered mercury-arc lamp. Typically, wet fluorescent magnetic particles define small discontinuities better than dry particles in visible light. Tests of these types are often used on piping, tubing, and weld root beads and completed fillet welds on steel structures. They also are used widely on jet engine turbine blades made of ferromagnetic materials, including some cobalt-base alloys. In other test systems, replication is made of the magnetic field patterns on flexible magnetic recording media. Magnetic recording techniques permit electronic imaging of defects, and provide records that can be stored, transmitted, or reproduced. Magnetic flux leakage tests have wide application in industrial inspection. Typical are tests of longitudinal welds in pipe during fabrication, and oil-field equipment, including oil-well drill pipe, tubing, line pipe, and structures. Pipelines are regularly inspected for thin wall using the magnetic flux leakage principle. Internal inspection devices called pigs are used for inspecting buried pipelines. Similar tests can be made on structures and piping in chemical plants and petroleum refineries.

4.6. Eddy Current Technique. When an alternating electric current (ac) flows in a coil of many turns of fine wire it generates an electric field with very little current flow. When such an energized coil is placed near the surface of a conducting material, eddy currents are induced in the material, see Figure 2. These currents are proportional to the electrical conductivity of the material. The induced current in the material flows in a direction opposite to the current in the coil. When current in the coil reverses in direction, the induced current reverses.

Material properties as well as defects such as cracks and voids, affect the magnitude and phase of the induced current. Analyzing the eddy currents the material conditions can be assessed. The primary advantage of this technique is that mechanical contact is not required between the eddy current transducers and the test object. Eddy current penetration depth can be controlled by adjusting the frequency of energizing current. The penetration depth of the eddy

current is related to the material resistivity, relative permeability and frequency in the following manner (1),

$$\alpha = 50.3\left(\frac{\rho}{\mu f}\right)^{1/2} \tag{2}$$

where α = depth of current penetration in mm, ρ = material resistivity (micro-Ω-cm), μ = dimensionless relative permeability, and f = frequency in Hz. The method has high sensitivity to small discontinuities at the surface and near the surface. Instrumentation for eddy current testing is relatively low cost for most applications. However, the main limitation of this technique is that its application is limited to the electrically conductive materials only. Interested readers are referred to Refs. (22–24).

4.7. Thermal Technique. In thermal techniques, the specimen is heated by a heat source and then the heat source is removed. The heat source can heat the specimen by radiation (heat lamp, lasers, etc), convection (blowers, ovens, etc), or conduction (contact hot plates, etc,). After some time a sensor scans the specimen and records its temperature. The temperature sensors can be contact or noncontact type. Noncontact sensors detect infrared (ir) radiation emanating from the test object. Two of the first publications in NDE using IR scanning and detection of flaws were by Florant (25) and Beller (26). If a homogeneous and uniform specimen surface is uniformly heated then the surface temperature at a given time during the cooling process should also be uniform. However, in presence of an internal flaw—inclusion, void, or crack—the surface temperature becomes different near the flaw and thus the flaw can be identified. Interested readers are referred to Refs. (27,28) where thermal inspection techniques have been discussed in greater detail.

4.8. Optical Holography. Holography is an exciting technique developed to obtain dramatic realism in photography. It also provides the capability for accurately measuring irregularities on the surface of a component. These irregularities often are caused by flaws beneath the surface and thus this technique sometimes can indirectly detect internal flaws. However, the technique does not penetrate the surface of opaque objects since the testing medium consists of light rays. The holographic process involves the recording of a complete wave front so that all of the information about a surface is retained and made available for subsequent retrieval. It is a two-step method. The first step is called formation or recording, the second step is called reconstruction that consists of placing the photographic film into a coherent beam of light and producing an image of the original object.

Optical holographic interferometry detects flaws in a material by recording measurements in unstressed and stressed conditions. Comparison of holographic fringes created on a hologram reveals flaws or discontinuities.

Various techniques are used in the construction of holograms. Three major hologram types are Fresnel holograms, Fraunhofer holograms, and Fourier holograms. Description of these three holography techniques can be found in Ref. (29). Modern holographic applications are not limited to optics, the method of

holography applies to all waves—electron waves, acoustic waves, X-rays, and microwaves.

4.9. Ultrasonic Technique. Ultrasonic waves are vibrational waves having frequencies higher than hearing range of the human ear, which is typically 20 kHz. The upper range of these waves can be as high as 15 or 30 GHz ($1\,\text{GHz} = 10^9\,\text{Hz}$). However, for most flaw detection applications the frequency generally varies from 200 kHz to 20 MHz. Ultrasonic techniques are useful for the internal flaw detection as well as for the material property determination. More information on the applications of ultrasonic techniques for material characterization can be found in Ref. (3). By ultrasonic techniques, flaw imaging in metals and nonmetals is possible, flaw distance from the surface can be measured, and material properties can be determined. When both surfaces of the object are not accessible then also ultrasonic techniques can be used. However, complex geometries are difficult to inspect by the conventional ultrasonic technique, small and tight or closed cracks are also difficult to detect by this method.

Basic Concepts. The speed of the wave propagation (C), frequency (f), and wave length (λ) are related in the following manner

$$\lambda = \frac{C}{f} \tag{3}$$

There are mainly two types of elastic waves—body or bulk waves and surface or guided waves—that propagate in a material. Body waves are of two types: longitudinal waves and shear waves. Longitudinal waves are also known as compressional wave, dilatational wave, acoustic wave, pressure wave, primary wave, or P-wave. Shear waves are called distortional wave, secondary wave or S-wave. Based on the polarization direction (vertical or horizontal) the S-wave can be classified as SV-wave or SH-wave.

Longitudinal wave speed (α) in a bulk material is given by (3),

$$\alpha = \sqrt{\frac{E(1-\nu)}{\rho(1+\nu)(1-2\nu)}} = \sqrt{\frac{\lambda + 2\mu}{\rho}} \tag{4}$$

where E = Young's modulus, ν = Poission's ratio, ρ = density, λ = Lame's first constant, and μ = Lame's second constant = shear modulus.

The shear wave speed β is given by

$$\beta = \sqrt{\frac{\mu}{\rho}} \tag{5}$$

where μ and ρ are identical to those in equation 4.

The surface wave, which is also known as the Rayleigh wave, propagates along the surface of a material and decays very fast with depth. It has a speed slightly smaller than the shear wave speed. The ratio C_R/β (C_R is the Rayleigh wave speed, and β is the shear wave speed) varies from 0.87 to 0.95 as the Poission's ratio varies from 0 to 0.5, as shown in Table 1.

Elastic waves that have plane wave fronts are called plane waves; similarly cylindrical and spherical waves have cylindrical and spherical wave fronts, respectively. In an infinite isotropic medium a point source generates spherical waves and a line source generates cylindrical waves. It can be shown from the Fourier analysis that both spherical and cylindrical waves can be mathematically reconstructed by superimposing a large number of plane waves propagating in different directions.

When a plane P- or S-wave strikes a plane interface between two linear elastic solids, then some of the elastic energy is reflected back and the rest is transmitted into the second material. Reflected and transmitted waves in general contain both P and S waves when a P- or S-wave strikes an interface between two solids. Thus in presence of a plane interface or boundary the propagating longitudinal waves can generate shear waves, and shear waves can generate longitudinal waves. This phenomenon is called "mode conversion". However, when a P-wave strikes an interface at 90° (wave propagation direction is normal to the interface plane), then reflected and transmitted energies contain only P-waves. Reflected and transmitted powers in this case are given by (3),

$$\frac{P_r}{P_i} = \left(\frac{Z_i - Z_2}{Z_i - Z_2}\right)^2 \qquad \frac{P_t}{P_i} = \frac{4Z_1Z_2}{(Z_1 + Z_2)^2} \tag{6}$$

where P_r, P_t, and P_i are reflected, transmitted and incident powers, respectively. Z_1 and Z_2 are acoustic impedances of materials 1 and 2, respectively. Acoustic impedance Z is the product of density (ρ) and P-wave speed (α), $Z = \rho\alpha$.

If a plane P-wave, propagating in material 1, strikes the interface of materials 1 and 2 at an angle θ_1, measured from the vertical line through the interface, then reflected S-wave makes an angle γ_1 and transmitted P- and S-waves in material 2 make angles θ_2 and γ_2 respectively, as shown in Figure 3. These angles are related to the P- and S-wave speeds of materials 1 and 2 in the following manner:

$$\frac{\sin\theta_1}{\alpha_1} = \frac{\sin\theta_2}{\alpha_2} = \frac{\sin\gamma_1}{\beta_1} = \frac{\sin\gamma_2}{\beta_2} \tag{7}$$

where subscripts 1 and 2 are used to indicate wave speeds in materials 1 and 2, respectively. Equation 7 is known as the Snell's law.

Experiment. Ultrasonic waves are generated by mechanical vibrations of piezoelectric crystals, excited by the electric current flow. Piezoelectric crystals are mounted in a casing with some damping material and protective coatings to build ultrasonic transducers. Detailed transducer design is beyond the scope of this chapter, however, interested readers can refer to Refs. (2,30,31) for more information.

Transducers generate uniform ultrasonic waves beyond the near field. Within the near-field the waves are not uniform, this phenomenon can be explained by Huygen's principle. For disk-shaped transducer elements with $\lambda \ll D$, the near field length N is approximately given by

$$N = \frac{D^2 - \lambda^2}{4\lambda} \approx \frac{D^2}{4\lambda} \tag{8}$$

where D is the diameter of the transducer and λ is the ultrasonic wave length. For full confidence in an ultrasonic inspection the specimen should be placed beyond the near field region.

The width of an ultrasonic beam increases as it propagates. This is a function of λ/D. The divergence angle (ϕ) of the beam can be calculated from

$$\phi = 2 \sin^{-1}\left(1.2\frac{\lambda}{D}\right) \tag{9}$$

For material inspection the ultrasonic transducers are used in one of the three common modes of operation; these are pulse-echoe mode, through-transmission mode and pitch-catch mode, see Figure 4. In the pulse-echoe mode the same transducer is used both as a transmitter and a receiver. In the through-transmission mode, two transducers are used—one transmits the signal and the second one receives the signal, the object under inspection is placed in between these two transducers. In the pitch-catch arrangement two transducers, one transmitter and one receiver, are used on the same side of the specimen. In presence of an internal defect the reflected signal changes. Therefore, analyzing the reflected signal the material can be assessed. For inspecting a specimen, the transducers generally move parallel to the specimen surface. At every position the transmitter sends the ultrasonic energy into the specimen, and the receiver receives the reflected or transmitted energy depending on the receiver orientation. When the transducers scan the specimen if the entire reflected/transmitted wave form is recorded at every position of the transducers and displayed on the oscilloscope screen then the recording system is called A-scan recording. However, in most applications only the peak value of the received wave form is recorded and plotted against the x, y coordinates of the receiver. In presence of a defect the peak value changes and thus the defective zone becomes prominant in the generated image. The ultrasonic image generated in this manner is called the C-scan image. Ultrasonic images of different horizontal cross sections at various depths of the specimen can be generated by recording the reflected signal at different time intervals or time gates. The vertical cross-sections of the horizontally placed specimen can be imaged by the B-scan recording. In this mode of recording the reflected signal strength is plotted against the time of arrival.

4.10. Acoustic Emission (AE) Technique. Here sensors (transducers) are used to listen to objects under inspection. If cracks are formed inside a material then acoustic energy is released because of the relaxation of the stress at the point of crack formation. The released acoustic energy propagates through the material to its surface, where it can be detected by the transducers mounted there. Therefore, formation or propagation of cracks inside the material can be identified. Besides the crack initiation and growth, other mechanisms that can produce acoustic emission are dislocation movements, twinning, phase changes, fracture of brittle inclusions or surface films, fiber breakage and delaminations in composite materials, chemical activity and cavitation. Emission energies due to

these disturbances can range from the motion of a few dislocations in metals to that required to cause catastrophic cracking of structures, such as during an earthquake. It is a passive technique, it simply listens to the sound generated inside the material because of some change occurring there. Therefore, it cannot detect a stable crack that is not growing. The crack size cannot be determined by this technique. Great sensitivity of the AE monitoring system sometimes presents problem if electrical interference and ambient noise are not properly filtered out of emission signals. The advantage of this technique is that since it is a passive system, no equipment is required to excite a pulse, and hence the instrumentation is relatively simple and inexpensive. Since the sensors can be located at remote locations these can be used when the object is in operation in hostile environments. A relatively large volume of material can be inspected at a reasonable cost, it is also suitable for long-term in-service monitoring. It can locate the crack initiation and growth points. These regions can then be inspected more carefully by other techniques such as ultrasonics and radiography to assess the material in those locations.

AE signals can be detected by accelerometers, piezoelectric transducers, air-gap capacitive transducers, optical/laser sensors, and magnetostriction transducers. This technique has been used in the past to give adequate warning before the catastrophic failure of 2014-T6 aluminum (32) and fiber-reinforced plastic composites (33). It is possible to distinguish the AE signals generated by fiber breakage, matrix cracking, and fiber delamination in composite materials and thus one can predict the type of damage created using this technique (34). In most materials, the number and intensity of the released acoustic signal increases significantly near the failure point. Therefore, it can serve as a good warning tool before the failure. AE technique has been found to be effective in detecting leaks in above-ground storage tanks (35,36) and in-flight monitoring of airplanes (37).

4.11. Acousto-Ultrasonics. This term was first used by Vary (38,39). Here, two piezoelectric sensors are attached to the surface of the specimen. One of the transducers, that acts as a source, is excited by an ultrasonic pulser. The other transducer acts as a sensor in a fashion typical of that used for acoustic emission monitoring. Thus this technique combines the ultrasonic excitation and AE monitoring. Although piezoelectric transducers are the most common type of excitation sources used in acousto-ultrasonic experiments several other types of excitation are also in use. Examples of such sources would include pencil lead breaks, breaking of glass capillaries, pulsed-laser excitation, the tapping of a hammer, and others. These excitations result in acoustic wave propagation within the object. The wave propagation within the object depends on the material properties of the object and the structure of the object. After these waves are detected by the acoustic receivers mounted on the surface of the object the data is analyzed to interpret the condition of the object. The main advantage of the acousto-ultrasonic technique over the acoustic emission technique is that stable cracks which are not growing can also be detected by this technique.

4.12. Moire Interferometry. The moire interferometry technique is used to measure displacement, rotation, curvature, and strain of a body. In this technique with the aid of some special patterns, known as the moire patterns, effects of the distortions of the body are magnified to provide a visual picture.

The term "moire" is a French word that means the patterns observed in watered silks. In moire interferometry the visual pattarns are produced by the superposition of two regular motifs that geometrically interfere. Regular motifs can be a set of equispaced parallel lines, rectangular arrays of dots, concentric circles, or equispaced radial lines. One needs to understand the basic theory of geometric moire to measure displacements and strains from the moire patterns formed by the moire interferometry. The theory of geometric moire is described in a simple manner in the following section. For a more detailed description of the geometric moire and the moire interferometry the readers are referred to Refs. (40,41).

Theory of In-Plane Moire. The most common use of moire patterns is to determine the displacements and strains of a plane parallel to the plane of analysis. In-plane moire patterns can be formed using very simple gratings, such as equispaced, parallel lines. If one plate remains fixed (reference motif or grating) and the other plate moves with the specimen (specimen motif or grating) then the interference pattern, formed by superimposing the two gratings, changes with the movement of the specimen grating. When the specimen grating moves, rotates, or deforms, then alternately dark and bright fringes are formed, as shown in Figure 5. These fringe patterns are called the moire patterns. In Figure 5, the line spacing in one grating (reference grating) has been kept unchanged in all four pictures but the other grating (specimen grating) has been subjected to a small rotation (top left), a large rotation (top right), a stretching (bottom left) and a combination of stretching and rotation (bottom right).

If the lines in individual patterns are equally spaced and the specimen movement is uniform then the fringes in the moire patterns are equally spaced also, as seen in Figure 5. The movement of the specimen can be determined from the angle of inclination of the fringes and the distance between the two dark or light fringes (pitch of the moire pattern).

Basic Equations. Let us consider two gratings of pitch (center to center distance between two successive lines) g and g'. If one grating rotates by an angle θ with respect to the other then it can be shown (40,42) that the moire patterns have a spacing of "d" between the two successive fringe lines and a slope of "ϕ" measured from the reference grating of pitch g. Both d and ϕ are related to g, g' and θ in the following manner.

$$d = \frac{gg'}{\sqrt{g^2 \sin^2 \theta + (g' - g \cos \theta)^2}} \qquad \tan \phi = -\frac{g \sin \theta}{g' - g \cos \theta} \tag{10}$$

Inverting the above relations one obtains

$$g' = \frac{d}{\sqrt{1 + (d/g)^2 + 2(d/g) \cos \phi}} \qquad \theta = \arctan \frac{\sin \phi}{d/g + \cos \phi} \tag{11}$$

In the above equations, g is known from the reference grating, d and ϕ can be measured from the moire patterns (43). Then g' and θ are obtained from equation 11. The parameter θ is a measure of the rotation of the specimen and

g' is a measure of the stretching of the specimen. After knowing g' the strain is obtained directly as

$$\epsilon = \frac{g' - g}{g} \tag{12}$$

From equation 10 one can see that for pure rotation since $g = g'$,

$$d = \frac{g}{2\ \sin(\theta/2)} \tag{13}$$

Clearly, for small rotations the denominator of the right-hand side of equation 13 is small, then d is large. Therefore, small rotations can be measured more accurately by moire patterns. Similarly for pure stretching ($\theta = 0$) equation 10 simplifies to

$$d = \frac{gg'}{g' - g} \tag{14}$$

Again for small stretching the denominator of the right-hand side of the above equation is small and thus d is large. Therefore, small strains can be measured more accurately than large strains using the moire patterns. For large θ or g' the spacing d becomes small and difficult to measure. For example when θ is 60° the spacing d is equal to g, for g' equal to $2g$ (100% strain) $d = 2g$. Clearly, if d is as small as g or $2g$ one cannot see it with the naked eyes or measure it accurately. In fact, for rotations that are $> 30^\circ$, and strains $> 30\%$ the moire fringe patterns disappear.

The moire pattern formed by horizontal gratings is a measure of veritcal displacements and the moire pattern formed by vertical gratings is a measure of horizontal displacements. If two moire patterns, both corresponding to horizontal displacements, are overlapped after giving one pattern a small uniform displacement in the horizontal direction then a new pattern is formed because of the interference between the two moire patterns. The new pattern is known as the super-moire and is a measure of the derivatives of displacements, or strains. If the original grating is in the x-direction and one moire pattern is given a shift in the x-direcion then the super-moire shows the variation of the strain ε_{xx}; if both these directions are y then the super-moire shows the variation of ε_{yy}, and if one direction (grating or shift) is x and the other is y then the super-moire is a measure of ε_{xy}.

Experimental Setup. To measure material deformation by the moire interferometry technique the specimen grating film is attached to the specimen. The reference grating is generated by interfering two laser beams infront of the specimen as shown in Figure 6. In the overlapping region of the two laser beams alternating dark and bright fringes are formed from the varying phase difference of the two arriving beams. A camera is placed in front of the specimen to photograph the combined effect of the two gratings. Due to the material deformation as the specimen grating moves with respect to the reference grating, the moire

pattern seen by the camera changes. From these moire patterns, photographed by the camera, the material deformation is obtained. A more rigorous description of the moire interferometry technique can be found in Refs. (41,44–46).

5. Recent Developments

In this section, nondestructive testing techniques that have been developed in recent years, are briefly described.

5.1. Lamb Wave Technique for Plate Inspection. Certain types of internal defects in multi-layered plates that cannot be seen very clearly by the conventional ultrasonic C-scan imaging technique can be detected easily when the plate is scanned by leaky Lamb waves (47–49). A leaky Lamb wave generated image is denoted as the L-scan image to distinguish it from the conventional C-scan image. Here L stands for the leaky Lamb wave. Chimenti and Martin (50) first attempted to generate the L-scan image with some success. The first step here is to place two transducers in a pitch-catch arrangement over the specimen to generate leaky Lamb waves in the specimen as shown in Figure 7. Chimenti and Martin (50) placed the receiver in the null zone and then they scanned the specimen. The null zone position changes in presence of an internal defect. Therefore, when a defect is encountered the receiver voltage amplitude is altered and the image of the defect is generated. The major problem with this arrangement is that the null zone position is very sensitive to the plate thickness. As a result, a small change in the plate thickness alters the receiver voltage amplitude significantly. To avoid this problem, one needs to filter the L-scan generated data through a special filter, called MFq filter, see Chimenti and Martin (50) for the detail description. This signal processing helps to minimize the effect of the plate thickness variation on the null zone but apparently retains the sensitivity to defects of interest. Kundu and co-workers (47), avoided the problem imposed by the variation in plate thickness, by placing the receiver beyond the null zone, as shown in Figure 7c. Thus only the propagating leaky Lamb waves reach the receiver. With this arrangement the investigators successfully detected certain types of internal defects in multilayered composite plates. Some of these defects, which could be seen clearly in L-scan images, were not very clear in C-scan images.

For efficiently generating the L-scan image one should first decide which leaky Lamb mode must be used. In presence of defects, such as broken fibers and delaminations, the stresses in the defective region are significantly reduced. Therefore, if these defects are located in a region where the stress level is high for certain propagating Lamb mode then those defects affect that mode by releasing the high stress level. This mode would then be most effective in producing the image of those defects. Therefore, stress levels inside the plate for various Lamb modes are to be first theoretically computed. For computing internal stresses in the plate one needs to study the mechanics of elastic wave propagation in a multi-layered solid. A number of investigators over last several decades have studied this problem (51–60) and that theory is not repeated here.

Experiment. The first step of generating an L-scan image is to produce propagating leaky Lamb waves in the specimen. For this purpose, two transducers

are placed in a pitch-catch arrangement over the plate specimen as shown in Figure 7,8**a**. The transmitter is excited by the tone burst excitation. The excitation frequency is then varied continuously from a minimum value to a maximum value within the band width of the transducers. The reflected signal is received by the receiver, the signal amplitude is then displayed on an oscilloscope screen as a function of the frequency. When the transmitter and the reflector are positioned such that the reflected energy is maximum or very close to maximum then the reflected amplitude spectrum has shapes as shown in Figure 7**a** or **b**. If no Lamb waves are generated then the spectrum looks like the plot shown in Figure 7**a** that has been generated by a couple of broad band 5-MHz transducers taking an aluminum block as the reflector, thus no Lamb waves are excited in the specimen. However, if leaky Lamb waves are generated at some frequencies then at those frequencies dips are observed, as shown in Figure 7**b**, which is produced by the same set of transducers at the same orientation but the aluminum block is replaced by a thin composite plate, where leaky Lamb waves are excited at some frequencies. If the transducers are moved further down, ie, the specimen-transducer distance is reduced without altering the distance between the two transducers then, because of defocusing, the reflected amplitude spectrum changes its shape and magnitude. In this defocused position, peaks are observed at frequencies that generate Lamb waves as shown in Figure 7**c**. This is because when the defocusing is high the specularly reflected beam cannot reach the receiver but the leaky Lamb waves can. That is why we observe peaks in Figure 7**c** at the frequency values for which we observed dips in Figure 7**b**. Hence, the frequencies corresponding to the leaky Lamb wave modes can be obtained from the dips (Fig. 7**b**) or peaks (Fig. 7**c**) of the reflected signal spectra. Then the leaky Lamb wave speed or the phase velocity can be obtained from Snell's law,

$$C_{\mathrm{L}} = \frac{\alpha_{\mathrm{U}}}{\sin\,\theta} \tag{15}$$

where C_{L} is the Lamb wave phase velocity, α_{U} is the longitudinal wave speed in the coupling fluid (for water it is equal to 1.49 km/s) and θ is the angle of inclination of the transducers, ie, the angle between the vertical axis and the transducer axis.

If the transducer angle is changed, corresponding leaky Lamb wave speed is changed, hence the dip positions along the frequency axis vary. Thus the Lamb wave dispersion curves can be experimentally generated by monitoring the transducer angles and dips of the reflected signal spectra. After selecting a specific leaky Lamb mode for scanning, that mode is generated by first setting the transducer angle (θ), then proper defocusing is done by vertically moving the transducers and observing the leaky Lamb wave peaks and finally the frequency is set at a value corresponding to a leaky Lamb wave peak of interest. The specimen is then scanned with this transmitter-receiver arrangement.

To illustrate the capability of Lamb waves in detecting internal defects in multi-layered composite plates, a specimen is scanned by two different leaky Lamb modes. This specimen is a five-layer metal matrix composite plate that has internal defects. The plate has a dimension of $80 \times 33 \times 1.97$ mm^3. Five

layers or plies of SCS-6 fibers in Ti-6Al-4V matrix are oriented in 0 and 90° directions in alternate layers. SCS fibers are produced by the Textron Inc. This fiber has a carbon core of ~25 μm diameter, two concentric layers of silicon carbide surround the carbon core and finally two very thin (couple of microns or so) layers of carbon coating are placed on the outside. The overall fiber diameter is ~152 μm. The fibers in the top, bottom, and middle layers are oriented in the 0° direction or along the length of the plate. The other two plies are in the 90° direction, or along the width of the plate. The composite is made by foil-fiber-foil technique. The internal flaws, shown in Figure 8**b**, are intentionally introduced in the plate during the fabrication process. The first and the fifth layers of fibers do not have any flaw. The left part of the second layer fibers (90°) is coated with boron nitride to impede the formation of good bonding between the fibers and the matrix as schematically shown in Figure 8. The fibers in the third layer (0°) are intentionally broken near the middle. The fourth layer (90°) has two areas of missing fibers. On the left side five fibers and on the right side 10 fibers are removed. The missing fiber zones have approximate widths of 1.2 and 2.4 mm on the left- and right-hand sides, respectively.

Figure 9 shows two L-scan images generated by leaky Lamb modes as described in the figure caption. Note that the top image of this figure clearly shows the missing fiber defects of the fourth layer while the bottom image shows delamination defect of the second layer. Two different frequency-phase velocity combinations of the striking beam produce two different stress profiles through the plate thickness; therefore, these two propagating waves have different degrees of sensitivity to the defects at various depths as can be seen in Figure 9. Readers are referred to Ref. 61 for a more comprehensive description of this problem.

Lamb wave inspection technique can be easily extended to large plate inspection applications where the specimen dimensions are much larger than small coupon specimens (3,62,63).

5.2. Cylindrical Guided Wave Technique for Pipe Inspection. The Lamb wave inspection technique for plates can be extended to pipe inspections by simply generating different modes of cylindrical guided waves in pipes and studying the interaction effects of these modes with different defects in the pipe.

Figure 10 shows two types of experimental setup for generating guided waves in pipes using solid and liquid coupling media (64). In Figure 10**a** the transmitter T is mounted on the spherical surface of a spherical/conical annular plexiglas coupler and receiver R is placed directly on the pipe wall. In Figure 10**b**, the pipe is placed underwater, the transmitter T is mounted on a frame and water is used as the coupler. The inclination angle of the transmitter can be changed in both arrangements for generating different guided wave modes.

To investigate the sensitivity of guided wave modes to pipe defects pipes with different types of defects are studied. The defects are placed between the transmitter and the receiver. Three aluminum pipe specimens are shown in Figure 11; these contain (**a**) no defect, (**b**) gauge, and (**c**) removed metal type defect. Note that pipes in Figure 11(**b**) and (**c**) have the same defect dimensions (width = 4.7 mm, depth = 0.56 mm), but they are formed differently. Gauge is formed by cold pressing, while the defect in Figure 11**c** is formed by machining. Two more defects (not shown in the figure)—a deeper machine cut

(width = 4.4 mm, depth = 0.62 mm) and a dent (width = 4.6 mm, depth = 0.76 mm) were also studied.

Received signal amplitudes, as a function of signal frequency or $V(f)$ curves, are plotted in Figure 12. Five curves are plotted in each figure for the five pipes—one is defect free and the remaining four are for the four defective pipes, described in the previous paragraph. The four defects are gouge, dent and machined grooves of two different depths marked by "reless" (less removed metal) and "remore" (more removed metal). Two peaks correspond to two different guided wave modes. Note that in Figure 12**a** there is hardly any difference between the signals generated by defective and defect-free pipes. However, as the signal incident angle is increased from 20 to 51° the $V(f)$ curves become more sensitive to the defects as seen in Figure 12**b**. Comparing Figure 12**b** and **c** it can be concluded that the signal sensitivity to defects increases further when the transducer arrangement shown in Figure 10**b** is used instead of that in Figure 10**a**.

Comparing the propagating modes with the dispersion curves it can be concluded that the modes that are generated near the horizontal asymptotes of the dispersion curves are more sensitive to defects. This observation was first reported by Guo and Kundu (65). This finding is important because it helps us to select the appropriate mode and the signal frequency to detect pipe defects efficiently.

In addition to pipe and plate inspection guided waves are also being used for detecting delamination between concrete and reinforcing bars and internal defects in concrete beams (66–72).

5.3. Acoustic Microscopy. Since the acoustic microscope was first introduced by Lemons and Quate (73) it has been used widely over the last three decades for different purposes. Material scientists used this apparatus for characterizing isotropic (74,75) and anisotropic materials (76–79). Development of line focus acoustic lenses (76,77) helped scientists to study material anisotropy by acoustic microscopes. Using this instrument, scientists also measured the coating thickness and its properties (80–82), characterized different types of bonds such as adhesive, diffusion and kissing bonds (83–86), detected surface and internal defects in metals and ceramic materials including semiconductors, ceramic capacitors, electronic packaging, electronic circuit boards and integrated circuit (IC) chips (87–91), obtained residual stress patterns (92), surface roughness (93), and plastic deformations (94,95) in materials. Different types of materials that have been characterized by this instrument include ceramics (96), polymers (97–99), composites (100,101), high temperature super conducting (HTSC) materials (102), fiber optics (103,104), rocks (105), and biological tissues and cells (106–111).

In addition to the inspection of solid and viscous materials, acoustic microscopes are also being used for characterizing some liquids that are used as the coupling fluid at the lens tip. It can measure sound velocity in a liquid very accurately (10 ppm) (112). Low temperature application of this instrument has been investigated also. Today a maximum resolution of 15 nm can be achieved by an acoustic microscope using a 15.3-GHz acoustic lens in the liquid helium coupling fluid near 0 K temperature (113–115). With this microscope one can image objects that show little or no contrast under a scanning electron

microscope. Conventionally acoustic microscopes are used to characterize surfaces and near surface regions, because it penetrates into the material a distance of the order of Rayleigh wavelength (116). To improve the penetration property of the acoustic microscope one can reduce the acoustic signal frequency (117–119). Low frequency (10–100 MHz) acoustic microscopes have been popular for many industrial applications.

Because of the wide range of applications of this instrument it has been extensively used in both materials engineering and medical science and >1000 research papers have been published on this subject. A comprehensive list of these works may be obtained from several review articles and books (120,121)

Working Principle. A schematic diagram of the acoustic microscope is shown in Figure 13**a**. The transducer T is mounted on the top of a lens rod, that is typically made of sapphire for high frequency (>100 MHz) or quartz for low frequency (<100 MHz) microscopes. Longitudinal ultrasonic waves are generated by the transducer T. The waves propagate through the lens rod and then are focused to a point (by a concave spherical lens located at the end of the lens rod) or to a line (by a concave cylindrical lens). When a specimen is placed between the lens and the focal point of the converging beams then the beams are reflected by the specimen and returns to the transducer after traveling through the coupling fluid and passing through the lens–fluid interface twice. The lens rod geometry is such that only two types of ultrasonic beams can return to the transducer. The beam that propagates along the central axis of the lens (marked by number 2 in Fig. 13**a**) do not deviate from its path and is reflected back to the transducer following the same path as shown in the figure. The beam 1 that strikes the specimen at the Rayleigh critical angle generates leaky Rayleigh waves along the coupling fluid-specimen interface and then goes back to the transducer (122–126). The transducer now works as a receiver, which receives two reflected beams having different phases. The phase difference between these two beams changes with the defocus distance, the distance between the lens focal point and the reflecting surface.

Depending on the phase difference between these two beams constructive or destructive interference may be resulted. Hence, the receiver voltage (V) versus the defocus distance (z) shows an oscillating pattern as shown in Figure 13**b**. This plot is commonly known as the $V(z)$ curve. Peaks and dips in the $V(z)$ curve corresponds to the constructive and destructive interference positions, respectively. The Rayleigh wave speed C_{R} in the specimen can be obtained from the spacing distance Δz in the following manner (122,125).

$$C_{\mathrm{R}} = \alpha_f \left[\frac{\alpha_f}{f\Delta z} - \left(\frac{\alpha_f}{2f\Delta z} \right)^2 \right]^{-1/2} \tag{16}$$

Where f is the signal frequency and α_f is the longitudinal wave speed in the coupling fluid.

Thus one elastic property (C_{R}) of the material can be easily obtained from the above equation. To obtain other properties such as P-wave speed, Young's modulus, ultrasonic attenuation coefficient, or film thickness one

needs to invert the complete $V(z)$ curve by simplex algorithm (81) or similar optimization techniques.

6. Concluding Remarks

Nondestructive evaluation is a service industry, and NDE economic activity is directly related to the economy of the basic industries, ie, aerospace, utilities, petrochemical, automotive, metals, or other (127). Overall, the NDE equipment market is small, totaling only $1 billion worldwide in 1990. The distribution of equipment sales among the various industrial groups is relatively equal. Aerospace is at the top with 26% of the market; petrochemical is at the bottom with 10%. Ultrasonic equipment dominates worldwide equipment sales; X-ray film and equipment also show strong markets. Eddy-current, magnetic particle, dye penetrant, and other techniques represent small portions of total sales. There are mixed forecasts for the future growth of NDE equipment sales. Growth in equipment sales may be tied to growth in the primary industries and the future of these industries is uncertain. Growth areas in NDE appear to be in equipment improvement and the development of new engineering systems for more efficient and reliable NDE. It is likely that the growth in NDE is shifting from a marketing oriented industry to one emphasizing engineering and education. NDE is seen to be moving to the role of a tool used by industry for economic benefit related to minimizing losses and maximizing income. Growth in the demand for NDE in engineering education is likely to continue (12).

Nondestructive evaluation requires specialized equipment, trained operators, and is an intrusion in operating or manufacturing schedule, which may involve considerable costs. The benefits may also be significant. Although the direct accountable benefit of NDE may be difficult to establish, a method for estimating benefit based on costs averted has been described (128). A return on investment case study for a power generating station reported significant savings a few years after the implementation of a nondestructive evaluation plan (129). Systematic NDE, used with maintenance procedures, decreased the energy lost at the power plant from cracked and leaking components. In implementing the NDE plan, the first effort was to attack the areas of greatest energy losses. It was only after several overhaul cycles that savings began to show. For this particular plant, an average cost of inspection for each boiler was $143,000 in 1989, a 23% increase over the 1979 inflation adjusted rate. Benefit, however, was realized when maintenance costs decreased from $10.97/MWh in 1979 to $4.34/MWh in 1989, the figures adjusted for inflation. Besides direct savings in reduced energy losses, savings also were realized in better schedules for repairs and maintenance as a result of the NDE plan.

BIBLIOGRAPHY

"Nondestructive Testing" in *ECT* 3rd ed., Vol. 16, pp. 47–72, by R. C. McMaster, The Ohio State University; "Nondestructive Evaluation" in *ECT* 4th ed., Vol. 17, pp. 259–287, by

Donald E. Bray, Texas A&M University; "Nondestructive Evaluation" in *ECT* (online), posting date: December 4, 2000, by Donald E. Bray, Texas A&M University.

1. D. E. Bray and D. McBride, *Nondestructive Testing Techniques*, John Wiley & Sons, Inc., New York, 1992.
2. D. E. Bray and R. K. Stanley, *Nondestructive Evaluation*, McGraw-Hill Book Co., Inc., New York, 1989.
3. T. Kundu, ed, *Ultrasonic Nondestructive Evaluation: Engineering and Biological Material Characterization*, CRC Press, Boca Raton Flor., 2003.
4. T. Kundu, Chapter 12, in *Modeling in Geomechanics*, M. Zaman, G. Gioda, and J. Booker, John Wiley & Sons, Inc., 2000, p. 267.
5. ASM International, *Metals Handbook*, Vol. 17, 9th ed., ASM International, Materials Park, Ohio, 1989.
6. R. C. McMaster, ed., *Nondestructive Testing Handbook*, The Ronald Press Co., New York, 1959, 1963, The American Society for Nondestructive Testing, Columbus, Ohio, 1979, p. 1977.
7. W. J. McGonnagle, *Nondestructive Testing*, 2nd ed., The American Society for Nondestructive Testing, Columbus, Ohio, 1969.
8. R. Halmshaw, *Non-destructive Testing*, Edward Arnold, London, 1987.
9. R. N. Pangborn, C. E. Bakis, and A. E. Holt, *J. Pressure Vessel Technol.* **113**, 163 (1991).
10. R. D. Barer and B. F. Peters, *Why Metals Fail*, Gordon and Breach, Science Publishers, New York, 1970.
11. *Source Book in Failure Analysis*, American Society for Metals, Metals Park, Ohio, 1974.
12. F. R. Hutchins and P. M. Unterweiser, *Failure Analysis: The British Engine Technical Reports*, American Society for Metals, Metals Park, Ohio, 1981.
13. G. T. Yonemura, *Considerations and Standards for Visual Inspection Techniques*, NBS1R76-1142, National Bureau of Standards, Washington, D.C., 1976.
14. R. C. McMaster, ed., "Liquid Penetrant Inspection," *Nondestructive Testing Handbook*, Vol. 2, 2nd ed., American Society for Nondestructive Testing, Columbus, Ohio, and the American Society for Metals, Cleveland, Ohio, 1982.
15. J. S. Borucki, and G. Jordan, *Metals Handbook*, Vol.17, 9th ed., ASM International, Materials Park, Ohio, 1989, p. 71.
16. R. Halmshaw, *Industrial Radiography*, Applied Science, London, 1982.
17. P. McIntire and L. Bryant, *Nondestructive Testing Handbook*, Vol. 3, 2nd ed., *Radiography and Radiation Testing*, American Society for Nondestructive Testing, Columbus, Ohio, 1985.
18. C. P. Slichter, *Principles of Magnetic Resonance*, Springer-Verlag, New York, 1980.
19. W. V. House and P. C. Lauterbur, *Nuclear Magnetic Resonance Zeugmatography Imaging*, 356/SPIE, Vol.173, *Application of Optical Instrumentation in Medicine VII*, 1979.
20. G. A. Matzkanin, *Investigation of the Effect of Moisture on the Mechanical Properties of Organic Matrix Composite Materials Using Nuclear Magnetic Resonance*, AVRAD-COM Report No. TR-81-F-5, Contract No. DLA 900-79-C-1266, 1981.
21. S. Bennett and L. Swartzendruber, *Metals Handbook*, Vol. 10, 9th ed., ASM International, Materials Park, Ohio, 1986, pp. 277–286.
22. J. L. Fisher, *Metals Handbook*, Vol. 17, American Society for Metals, Metals Park, Ohio, 1989, p. 195.
23. Materials Evaluation, *Special Issue on Remote-Field Eddy Current Testing* **47** (1989).

24. Materials Evaluation, *Special Issue on Remote-Field Eddy Current Testing* **49** (1991).
25. L. Florant, *Inst. Soc. Am.* **11**, 61 (1964).
26. W. Beller, *Missiles-Rockets* **16**, 22 (1965).
27. W. D. Lawson and J. W. Sabey, *Research Techniques in Nondestructive Testing*, Vol 1, Chap. 14, Academic Press, London, 1970, p. 443.
28. G. Hardy, and J. Bolen, *Thermal Inspection, in Metals Handbook*, 9th ed., *Nondestructive Testing and Quality Control*, Vol. 17, ASM International, Materials Park, Ohio, 1989.
29. H. J. Caulfield, *Handbook of Optical Holography*, Academic Press, New York, 1979.
30. J. Krautkramer and H. Krautkramer, *Ultrasonic Testing of Materials*, 3rd ed. Springer-Verlag, Berlin, 1983.
31. M. G. Silk, *Ultrasonic Transducers for Nondestructive Testing*, Adam Hilger, Bristol, 1984.
32. C. E. Hartbower, W. G. Reuter, C. F. Morais, and P. P. Crimmins, *Correlation of Stress Wave Emission Characteristics with Fracture in Aluminum Alloys*, Aerojet Solid Propulsion Company, 1971.
33. J. R. Mitchell, J. R. , *FRP Storage Tank Testing with Acoustic Emission*, Plastics Seminar, Technical Report TR-107-69, 55, Physical Acoustics Corp., Princeton, NJ, 1981.
34. A. Mal, F. J. Shih, and W. H. Prosser, in T. Kundu, ed. *Ultrasonic Methods for Material Characterization*, Vol. 3, Special Issue of the I2M (Instrumentation, Measurement and Metrology) Lavoisier, Paris, 2003, p. 11.
35. R. K. Miller, *Mater. Eval.* **48**, 822, 826, 829 (1990).
36. R. Nordstrom, *Mater. Eval.* **48**, 251 (1990).
37. G. C. Martin, *In-Flight Acoustic Emission Monitoring, Conf. Proc. Mechanics of Nondestructive Testing*, Blacksburg, Va, 1980.
38. A. Vary, in J. C. Duke, ed., *Acousto-Ultrasonic: Theory and Application*, Plenum Press, New York, 1988, pp. 1–21.
39. A. Vary and K. J. Bowels, *Polym. Eng. Sci.* **19**, 373 (1979).
40. V. J. Parks, Chap. 6, *Handbook on Experimental Mechanics*, 2nd ed., A. S. Kobayashi, ed., VCH Publishers, New York, 1993, p. 267.
41. D. Post, in A. S. Kobayashi ed., *Handbook on Experimental Mechanics*, 2nd ed., Chapt. 7, VCH Publishers, Inc., New York, 1993, p. 297.
42. F. P. Chiang, in A. S. Kobayashi, ed. *Manual of Engineering Stress Analysis*, 3rd ed. Chapt. 6, Prentice-Hall, Englewood Cliffs, N.J., 1982.
43. A. J. Durelli and V. J. Parks, *Moire Analysis of Strain*, Prentice-Hall, Englewood Cliffs, N.J., 1970.
44. D. Post, *Opt. Eng.* **24**, 663 (1985).
45. C. A. Scimmarella, *Exp. Mech.* **22**, 418 (1982).
46. P. S. Theocaris, *Moire Fringes in Strain Analysis*, Pergamon Press, Elmsford, N.Y., 1969.
47. T. Kundu, K. Maslov, P. Karpur, T. E. Matikas, and P. D. Nicolaou, *Ultrasonics* **34**, 43 (1996).
48. T. Kundu and K. Maslov, *Int. J. Solids Struct.* **34**, 3885 (1997).
49. K. Maslov and T. Kundu, *Ultrasonics* **35**, 141 (1997).
50. D. E. Chimenti and R. W. Martin, *Ultrasonics* **29**, 13 (1991).
51. W. T. Thomson, *J. Appl. Phys.* **21**, 89 (1950).
52. N. A. Haskell, *Bull. Seismolog. Soc. Am.* **43**, 17 (1953).
53. J. W. Dunkin, *Bull. Seismolog. Soc. Am.* **55**, 335 (1965).
54. F. Schwab, F. and L. Knopoff, *Bull. Seismolog. Soc. Am.* **60**, 321 (1970).
55. T. Kundu and A. K. Mal, *Wave Motion* **7**, 459 (1985).

56. A. K. Mal, *Wave Motion* **10**, 257 (1988).
57. A. K. Mal, C.-C. Yin, and Y. Bar-Cohen, *Comp. Eng.* **1**, 85 (1991).
58. D. Lévesque and L. Piché, *J. Acous. Soc. Am.* **92**, 452 (1992).
59. L. M. Brekhovskikh and O. A. Gobin, *Acoustics of Layered Media, Plane and Quasi Plane Waves*, Springer-Verlag, New York, 1990.
60. M. Castings and B. Hosten, *J. Acous. Soc. Am.* **95**, 1931 (1994).
61. T. Kundu, C. Potel, and J. F. de Belleval, *Ultrason.* **39**, 283 (2001).
62. T. Ghosh and T. Kundu, *J. Acous. Soc. Am.* **104**, 1498 (1998).
63. T. Ghosh, T. Kundu, and P. Karpur, *Ultrasonics* **36**, 791 (1998).
64. W. B. Na and T. Kundu, *ASME J. Pressure Vessel Techno.* **124**, 196 (2002).
65. D. Guo and T. Kundu, *J. Acous. Soc. Am.* **110**, 303 (2001).
66. W. B. Na and T. Kundu, *J. Exp. Mech.* **43**, 24 (2003).
67. W. B. Na, T. Kundu, and M. Ehsani, *Mater. Eval.* **61**, 155 (2003).
68. W. B. Na, T. Kundu, and M. Ehsani, *Computer-Aided Civil Infrastruct. Eng.* **18**, 57 (2003).
69. Y.-C. Jung, T. Kundu, and M. R. Ehsani, *ACI Mater. J.* **99**, 292 (2002).
70. W. B. Na and T. Kundu, *J. Acous. Soc. Am.* **111**, 2128 (2002).
71. W. B. Na, T. Kundu, and M. Ehsani, *Mater. Eval.* **60**, 437 (2002).
72. Y. C. Jung, T. Kundu, and M. Ehsani, *Mater. Eval.* **59**, 418 (2001).
73. R. A. Lemons and C. F. Quate, *A Scanning Acoustic Microscope*, Proceedings of the IEEE Symposium, Vol. 18, 1973.
74. A. Atalar, *J. App. Phy.* **50**, 8237 (1979).
75. G. A. D. Briggs, C. Illett, and M. G. Somekh, in E. A. Ash and C. R. Hill, eds., *Acoustical Imaging*, Plenum Press, London, Vol. 12, 1982, p. 89.
76. J. Kushibiki, A. Ohkubo, and N. Chubachi, *Acoust. Imaging* **12**, 101 (1982).
77. J. Kushibiki, H. Takahashi, T. Kobayashi, and N. Chubachi, *App. Phys. Lett.* **58**, 2622 (1991).
78. J. A. Hildebrand and L. K. Lam, *Appl. Phys. Lett.* **42**, 413 (1983)
79. J. O. Kim, J. D. Achenbach, P. B. Mirkarimi, M. Shinn, and S. A. Barnett, *J. Appl. Phys.* **72**, 1805 (1992).
80. R. D. Weglein and A. K. Mal, *Surface and Coatings Technol.* **47**, 677 (1991).
81. T. Kundu, *J. Acous. Soc. Am.* **91**, 591 (1992).
82. Z. Yu, and S. Boseck, *Optik* **96**, 83 (1994).
83. C. P. Slichter, *Principles of Magnetic Resonance*, Springer-Verlag, New York, 1980.
84. B. Derby, G. A. D. Briggs, and F. E. Wallach, *J. Mater. Sci.* (GB) **18**, 2345 (1983).
85. J. Cognard, S. Sathish, A. Kulik, and G. Gremaud, *J. Adhes. Sci. Technol.* **32**, 45 (1990).
86. P. B. Nagy, *J. Adhesion Sci. Tech.* **5**, 619 (1991).
87. R. D. Weglein, *IEEE Trans. Sonics Ultrason.* **SU-30**, 40 (1983).
88. A. J. Miller, *IEEE Trans. Sonics Ultrason.* **SU-30**, 313 (1983).
89. C. W. Lawrence, C. B. Scruby, G. A. D. Briggs, and A. Dunhill, *NDT International* **23**, 3 (1990).
90. T. M. Moore, *Solid State Phys.* **35**, 411 (1992).
91. G. De Liso, M. Muschitello, and M. Stucchi, *Scanning* **15**, 236 (1993).
92. S. W. Meeks, D. Peter, D. Horne, K. Young, and V. Novotny, *Appl. Phys. Lett.* **55**, 1835 (1989).
93. K. Gopalan, R. A. Roberts, J. G. Markovich, and J. J. Vaitekunas, *IEEE Instrumentation and Measurment Technology Conf.*, IEEE Piscataway, New Jersey, 1989, p. 54.
94. I. Ishikawa, T. Semba, H. Kanda, K. Katakura, Y. Tani, and H. Sato, *IEEE Trans. Ultrason. Ferroelectric Freq. Controls* **36**, 274 (1989).
95. J. M. R. Weaver and G. A. D. Briggs, *J. Phys.* **12**, 743 (1985).

96. L. R. Clarke, C.-H. Chou, B. T. Khuri-Yakub, and D. B. Marshall, *IEEE Ultrasonic Symposium*, New York, 1985, p. 979.
97. P. A. Tucker and R. G. Wilson, *J. Polym. Sci.* **18**, 97 (1980).
98. R. G. Maev, *Arch. Acous.* **12**, 13 (1988).
99. A. F. Fagan, J. M. Bell, and G. A. D. Brigg, in A. C. Roulin-Moloney, *Fractography and Failure Mechanisms of Polimers and Composites*, Elsevier, Applied Science, 1989, p. 213.
100. M. R. Karim, and T. Kundu, Twelfth Annual Energy Sources Technolgy Conference and Exhibition, Houston, Texas, Jan.22-25, 1989, ASME Petroleum Division, Vol.PD-**24**, 1989, p. 131.
101. C. W. Lawrence, C. B. Scruby, and G. A. D. Briggs, *J. Mater. Sci.* **28**, 3635 (1993).
102. A. Bukhny, L. A. Chernosatonskii, and R. G. Maev, *J. Microsc.* **160**, 299 (1990).
103. C. K. Jen, C. Neron, J. F. Bussiere, L. Li, R. Lowe, and J. Kushibiki, *Appl. Phys. Lett.* **55**, 2485 (1989).
104. A. Gadomski and C. Boseck, *Opt. Appl.* **20**, 303 (1990).
105. A. Rodriquez, G. A. D. Briggs, and M. Montoto, *J. Microsc.* **160**, 21 (1990).
106. C. J. Pavlin, M. D. Sherar, and S. Foster, *Ophthamology* **97**, 244 (1990).
107. G. Scherba, P. A. Hoagland, and D. O. O'Brian, *IEEE Trans. Ultrason. Ferroelectric Freq. Controls* **41**, 451 (1994).
108. T. Kundu, J. Bereiter-Hahn, and K. Hillmann, *Biophys. J.* **59**, 1194 (1991).
109. T. Kundu, J. Bereiter-Hahn, and K. Hillmann, *J. Acoust. Soc. Am.* **91**, 3008 (1992).
110. T. Kundu, J. Bereiter-Hahn, and I. Karl, *Biophys. J.* **78**, 2270 (2000).
111. C. Jorgensen and T. Kundu, *J. Orthope. Res.* **20**, 151 (2002).
112. F. Guillon, *Ultrasonics* **27**, 26 (1989).
113. D. Rugar, J. S. Foster, and J. Heiserman, in E. Ash and C. R. Hill, eds., *Acoustical Imaging*, Vol. 12, Plenum Press, New York, 1982, p. 13.
114. B. Hadimioglu and J. S. Foster, *J. Appl. Phys.* **56**, 1976 (1984).
115. A. A. Moulthrop, M. S. Muha, B. Hadimioglu, C. P. Silva, and G. C. Kozlowski, *IEEE Trans. Ultrason. Ferroelect. Freq. Control* **39**, 204 (1992).
116. A. Atalar, *IEEE Trans. Sonics Ultrasonics* **32**, 164 (1985).
117. R. S. Gilmore, K. C. Tam, J. D. Young, and D. R. Howard, *Phil. Trans. R. Soc.* **320**, 215 (1986).
118. T. Kundu, *J. Appl. Phys. B.: Photophys. Laser Chem.* **46**, 325 (1988).
119. M. A. Awal, A. Mahalanobis, and T. Kundu, *J. Nondestr. Eval.* **11**, 19 (1992).
120. G. A. D. Briggs, *Acoustic Microscopy*, Oxford University Press, 1992.
121. B. T. Khuri-Yakub, *Ultrasonics* **31**, 361 (1993).
122. R. D. Weglein, *Appl. Phys. Lett.* **34**, 179 (1979).
123. H. L. Bertoni, *IEEE Trans. Son. Ultrason.* **31**, 116 (1984).
124. T. Kundu, A. K. Mal, and R. D. Weglein, *J. Acoust. Soc. Am.* **77**, 353 (1985).
125. T. Kundu and A. K. Mal, *Int. J. Eng. Sci.* **24**, 1819 (1986).
126. T. Kundu, *ASME J. Appl. Mech.* **59**, 54 (1992).
127. R. K. Stanley, *Proceedings of the 13th World Conference on NDT*, Sao Paulo, Brazil, 1992.
128. C. Lopez, *Buyer's Guide, Mater. Eval.* **52**(6) (1993), (revised annually).
129. C. D. Wells, *Insight* **36**, 331 (1994).

T. KUNDU
University of Arizona

Table 1. **Variation of C_R/β with the Poission's Ratio ν**

ν	0.0	0.05	0.15	0.25	0.30	0.40	0.50
C_R/β	0.87	0.88	0.90	0.92	0.93	0.94	0.95

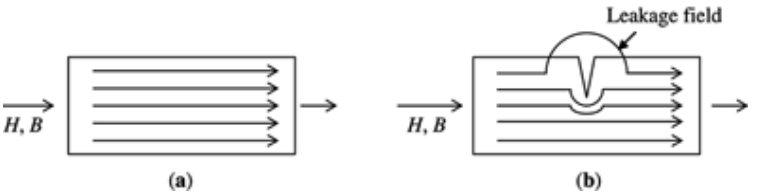

Fig. 1. Schematic of magnetic flux leakage tests where H, B represent an external applied magnetic field. See text. (**a**) Saturated material having no crack and (**b**) leakage field caused by crack.

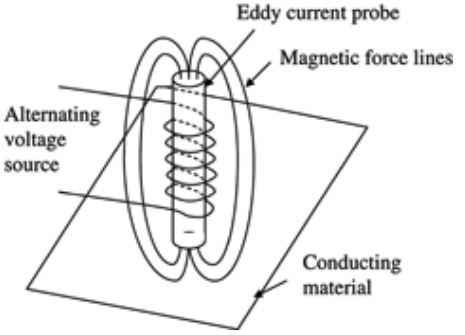

Fig. 2. Schematic of an eddy current probe placed near an electrically conductive material.

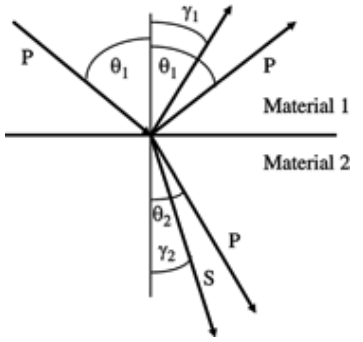

Fig. 3. Reflected and transmitted P- and S-waves generated by an incident plane P-wave at the plane interface of two solids.

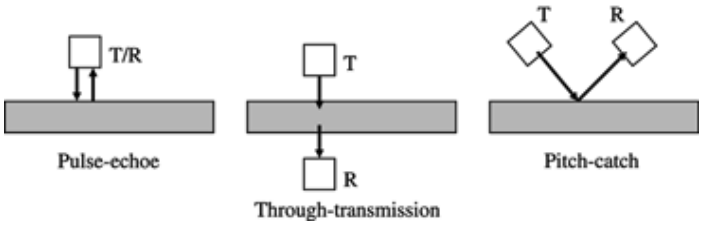

Fig. 4. Three modes of ultrasonic testing: T is transmitter and R is receiver.

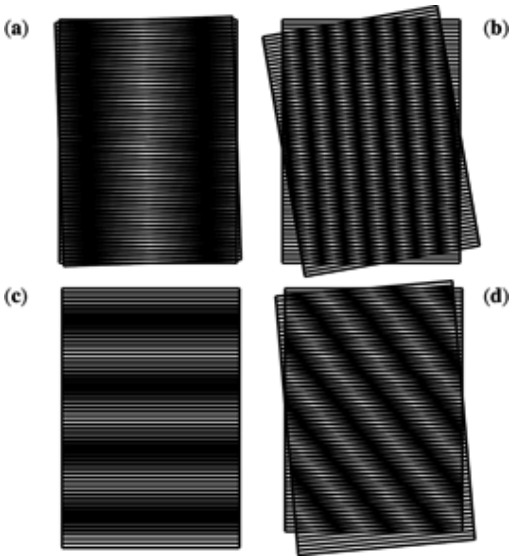

Fig. 5. Moire fringes generated by the superimposition of undeformed and deformed gratings. In the deformed grating the deformations are a small rotation (**a**), a large rotation (**b**), a stretching (**c**), and a combination of stretching and rotation (**d**).

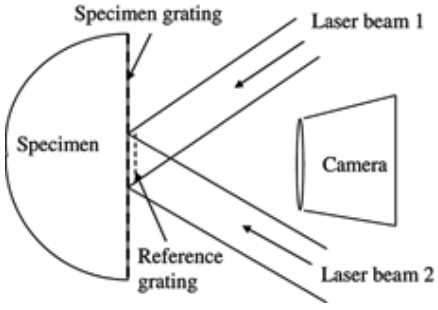

Fig. 6. Schematic of moire laser interferometry experimental set up.

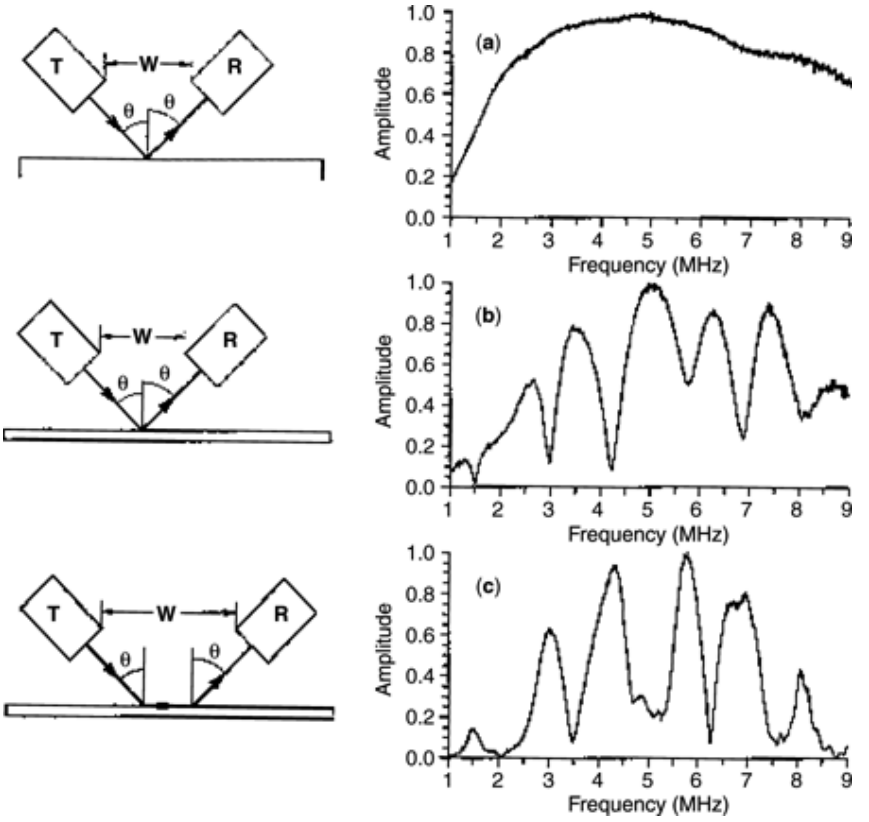

Fig. 7. Reflected wave spectra (right column) for different transmitter-receiver-specimen orientations shown in the left column. For a thick aluminum block reflector no Lamb waves are generated [plot (**a**)]; for a plate in the focus position [plot (**b**)] dips correspond to the leaky Lamb waves; for a plate in the defocus position [plot (**c**)] peaks correspond to the leaky Lamb waves (after Ref. 47).

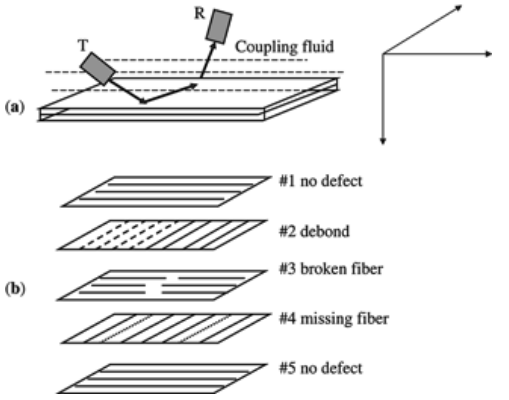

Fig. 8. (**a**) Relative orientations of the transmitter, receiver and the plate specimen, (**b**) Schematic of the internal defects in the five layers of the composite plate specimen (after Ref. 61).

Fig. 9. Two images of the five layer composite plate specimen generated by two different frequency-phase velocity combinations. The top image has been generated by 5.0-MHz signal incident at 20° and the bottom image has been produced by 5.15-MHz signal incident at 21° (after Refs. 47,49).

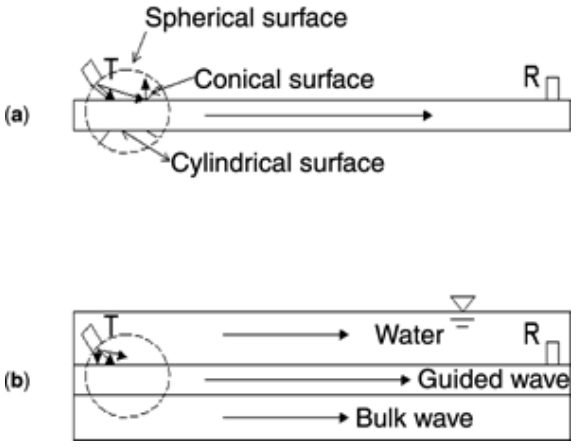

Fig. 10. Two settings for generating guided waves in pipes using solid and liquid coupling media (**a**) Transducer is on annular plexiglas holder when the pipe is not underwater. (**b**) Transducer is attached to the annular holder without Plexiglas coupler for underwater pipes.

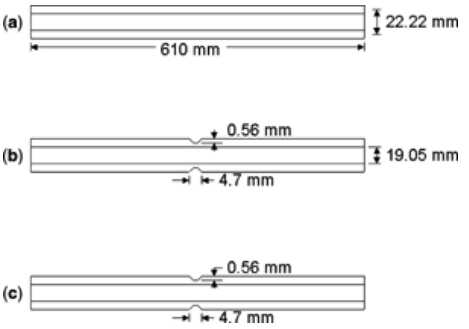

Fig. 11. Aluminum pipe specimen: (**a**) defect free; (**b**) gouge; (**c**) removed metal. All pipes have same length, outer radius, and inner radius (Ref. 64).

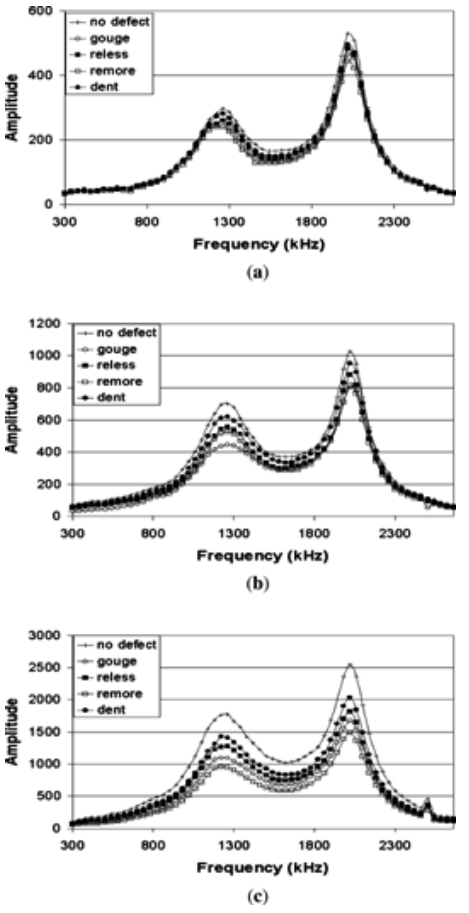

Fig. 12. *V*(*f*) curves for five different aluminum pipes for various arrangements (Ref. 64). (**a**) Transmitter-receiver arrangement is as shown in Figure 10**a**, and the transmitter angle is 20°. (**b**) Transmitter-receiver arrangement is as shown in Figure 10**a**, and the transmitter angle is 51°. (**c**) Transmitter-receiver arrangement is as shown in Figure 10**b**, and the transmitter angle is 51°.

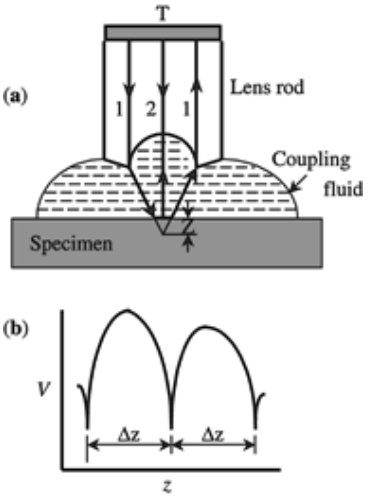

Fig. 13. (**a**) Schematic of an acoustic microscope. (**b**) A typical $V(z)$ plot.